physica status solidi pss a
www.pss-a.com

Effective Absorption Cross Sections of Defects in High Pressure High Temperature Diamond Studied by Modulated Surface Photovoltage Spectroscopy

*Steffen Fengler, Ilya Ponomarev, and Thomas Dittrich**

It has been shown on the example of high pressure high temperature (HPHT) diamond samples that effective absorption (or photogeneration) cross sections of defect states can be obtained by fitting modulated surface photovoltage (SPV) spectra. Spectra of in-phase and phase-shifted by 90° SPV signals were measured without and with bias light at different wavelengths. In the fits, positive and negative features in the SPV spectra have been considered low and independent. Values of absorption energies and broadening parameters of up to 10 defect-related transitions were obtained for two rather different HPHT diamond samples. The influence of the phase of SPV signals and of bias light on the analyzed parameters is briefly discussed. Theresults demonstrate the opportunity of precise analysis of complex SPV spectra over the entire bandgap of diamond. The general applicability of the developed fitting procedure has been shown for precise fitting of absorption spectra below the bandgap of diamond.

1. Introduction

Defect states in the bandgap of diamond ($E_g = 5.47$ eV)[1] play a decisive role for future applications in power electronic (see, for example,),[2–5] radiation detectors,[6] quantum sensors,[7] or photocatalysts.[8] There are two major approaches currently in use to produce synthetic diamonds-chemical vapor deposition (CVD) from low pressure gas reactants and a temperature gradient method under high pressure and high temperature (HPHT). Each method has its advantages and disadvantages, which define the areas of applications. HPHT diamond growth is near the equilibrium process, and by its nature, it allows diamonds to grow of the highest crystalline quality. CVD diamond growth technology is particularly useful for electronic applications since it allows to control contents of impurity atoms and dopants by using high purity gas precursors and appropriate chamber materials, as well as by optimizing growth conditions. A drawback of the CVD diamond growth is that it is an essentially non-equilibrium process making the control of intrinsic defects more difficult. As a result, CVD grown crystals typically have internal strain (that can be easily observed in cross-polarized light) and densities of dislocation on the order 10^3–10^6 cm^{-2}.

HPHT diamonds exhibit distinct bandgap defects compared to CVD substrates, primarily due to differences in growth mechanisms and impurity incorporation pathways. Type IIa HPHT diamonds are characterized by catalyst-derived atomic impurities (Ni, Co, and Si) forming sector-localized defects like [Si–V]$^-$ and nickel centers, whereas CVD diamonds exhibit vacancy-dominated defects from gas-phase precursors. This distinction is critical for applications in quantum sensing and electronics, where defect engineering dictates performance.

For numerous applications, HPHT,[9] diamond plays an important role. Defects in the bandgap of diamond are usually studied by absorption and luminescence spectroscopies,[10] which demand a considerable amount of absorbing species or radiative recombination, respectively. For a deeper understanding of the origin of defect states and their dependence on technological processes, relatively fast and more universal characterization methods of defect states are desired. Surface photovoltage (SPV) methods provide information about electronic transitions in diamond and do not require contact preparation.[11,12] However, a more detailed analysis of SPV spectra is usually not straightforward, for example, due to a variable dependence of SPV signals on generation rate and/or due to a dynamic overlap of positive and negative SPV signals measured subsequently in a spectrum. For these reasons, transition energies of defect states are traditionally obtained at onset energies where the slopes of SPV spectra change. The approach of the analysis of onset energies does not allow for a detailed analysis, for example, of effective absorption cross sections (σ_{abs}) of defect states. In this work, we show that effective absorption cross sections of defect

S. Fengler
Freiberg Instruments GmbH
Delfter Str. 6, 09599 Freiberg, Germany

I. Ponomarev
Euclid Beamlabs, LLC
10000 Virginia Manor Rd, Ste 330, Beltsville 20375, Maryland, USA

T. Dittrich
Helmholtz-Zentrum Berlin für Materialien und Energie GmbH
Schwarzschildstr. 8, 12489 Berlin, Germany
E-mail: dittrich@helmholtz-berlin.de

The ORCID identification number(s) for the author(s) of this article can be found under https://doi.org/10.1002/pssa.202500531.

DOI: 10.1002/pssa.202500531

states in diamond can be deduced from modulated SPV spectra by fitting.

In modulated SPV spectroscopy, light from a monochromator hits the sample during the first half of the modulation period (T_{mod}) while the light is switched off during the second half (see also Figure S1, Supporting Information). The evolution and relaxation of SPV signals in diamond usually last over time ranges longer than typical modulation periods, which are of the order of tens to hundreds of ms. In this sense, a modulation can be considered as a disturbance between two nonequilibrium states. Consequently, modulated SPV signals of diamond are usually rather low (μV...mV range) in modulated SPV spectroscopy. Therefore, modulated SPV signals fulfill the condition of the low signal case, i.e., modulated SPV signals are proportional to the photogeneration rate, which is proportional to the photon flux (Φ) and σ_{abs}. In addition, it is reasonable to suppose that positive and negative SPV signals originate from independent processes, i.e., modulated SPV spectra can be considered as a linear superposition of independent spectral contributions from different defect states. Incidentally, prolonged diffusion processes, for example, can lead to spectral contributions that depend on each other.

Alkauskas, McCluskey, and Van de Walle followed the treatment of Kopylov and Pikhtin and got the following expression for σ_{abs}[13]

$$\sigma_{abs}(h\upsilon) \propto \int_0^{\infty} \frac{\exp[-(E + E_{abs} - h\upsilon)^2/\Gamma^2] \cdot \sqrt{E} \cdot dE}{h\upsilon \cdot (E + E_{abs})^2} \quad (1)$$

where $h\upsilon$, E_{abs}, and Γ denote the current photon energy in the spectrum, the energy of the sharp absorption onset at the temperature of 0 K and the broadening parameter.

In this work, measured spectra of modulated in-phase (X) and phase-shifted by 90° (Y) SPV signals were fitted by using Equation (1), considering the sign ($P = -1, +1$) and the amplitude (A_i) and using the spectra of Φ($h\upsilon$) and of the dispersion ($D(h\upsilon)$)

$$SPV_{sim}(h\nu) = \phi(h\upsilon) \cdot D(h\upsilon) \cdot \sum_{i=1}^{n} [P_i \cdot A_i \cdot \sigma_{abs,i}(E_{abs,i}, \Gamma_i)] \quad (2)$$

where i is the number of a certain defect transition characterized by $\sigma_{abs,i}$ which is given by $E_{abs,i}$ and Γ_i regarding to Equation (1), and n is the total number of defect states in a spectrum.

An amplitude characterizing directly the absorption cross section cannot be obtained since the amplitude depends on the charge separation length, i.e., the distance between the centers of separated positive and negative charges, which is uncertain, and which depends on the mechanisms of charge separation and relaxation and on the location of defect states in a sample. Therefore, an effective absorption cross section of a defect transition i ($\sigma_{abs,eff,i}$) is introduced

$$\sigma_{abs,eff,i}(E_{abs,i}, \Gamma_i, A_i) = A_i \cdot \sigma_{abs}(E_{abs,i}, \Gamma_i) \quad (3)$$

HPHT diamond is known for a wide range of defects. Here, the effective absorption cross sections of two HPHT diamond samples with very different densities of impurities were obtained. Furthermore, absorption spectra of different types of diamond were precisely fitted with the developed procedure below the bandgap of diamond.

2. Experimental Section

Two Type IIa HPHT (100) multisectorial samples (EB1 and EB2), grown at Euclid Beamlabs with different growth conditions, were investigated. Their characteristics are shown in **Table 1**. Optical images of both samples in visible, cross-polarized, and deep UV light are shown in **Figure 1**a–f. Both samples were strain-free without any signs of birefringence.

The nitrogen concentration was less than 1000 ppb for sample EB1 and less than 50 ppb for sample EB2. The areas of samples EB1 and EB2 were larger than the diameter of the perforated electrode. The thicknesses were 0.3 and 0.5 mm for samples EB1 and EB2, respectively. In contrast to sample EB2, sample EB1 was grown with nickel in the metal catalyst.

Figure 1c and d show images under illumination with cross-polarized light, allowing macroscopic (>10 μm) metallic inclusions inside a diamond matrix. A nonoptimal fast HPHT growth (sample EB1) results in an increased probability of metal capture within the diamond. Therefore, we can expect larger amounts of related defects in sample EB1.

Many atomic defects in diamond, especially point defects such as nitrogen-vacancy (NV) centers, are often concentrated at boundaries between growth sectors. Growth sectors emerge during the HPHT crystal growth process. Under illumination with deep ultraviolet (DUV) light at photon energies above 5.51 eV (about 225 nm), growth sectors can be separated by distinct fluorescence patterns because defect densities can be different in different growth sectors. DiamondView (de Beers Group) fluorescence images under exposure in DUV light (about 225 nm) reveal different growth sectors in the samples (Figure 1e and f). Sample EB1 (Figure 1e) showed a multisectorial nature across the whole sample, whereas sample EB2 had a large (100) growth sector in the center (large dark area) and (111) growth sectors near the edges.

Modulated SPV spectra were measured in the same regime and set-up described recently.[14] In this set-up, a laser driven light source (Hamamatsu, EQ-99X) with an illumination unit, a mirrorless double prism monochromator (DPM100,)[14] and an outcoupling unit (Freiberg Instruments) are used for illumination of the sample through a fine perforated front electrode (diameter 7 mm). The optical chopper was set in the outcoupling unit just behind the exit slit of the monochochromator so that the diameter of the light spot was small in comparison to the half-period path at the distance of the light spot to the rotation axis of the chopper wheel (see also Figure S1, Supporting Information). The chopper frequency was set to 8 Hz. Modulated transients were measured after switching on and off illumination between 0 and 62.5 ms (light on) and 62.5 and 125 ms (light off), whereas the uncertainty in the switching times was about 1...2 ms due to the dimension of the light spot in the plane of the chopper blade. Transients were averaged over 40 periods. Measurements were performed without bias illumination and under bias illumination with defocused laser diodes of 650, 532, and 405 nm (intensities 3.6, 0.55, and 33 mW, respectively).

Table 1. Characteristics of the diamond samples investigated.

ID	Type	Growth	Orientation, shape and size [mm^3]	Content of B and N [ppb]	Defect density [cm^{-2}]
EB1	IIa HPHT	Standard metal catalyst with Ni, fast growth, metallic inclusions present	(100), polygon 13 × 12.5 × 0.3	[B] < 50 [N] < 1000	>50
EB2	IIa HPHT	High purity slow growth with nitrogen getterers (Ca,Ti) in the metal catalyst	(100) with miscut, square 8 × 8 × 0.5	[B] < 10 [N] < 50	<10

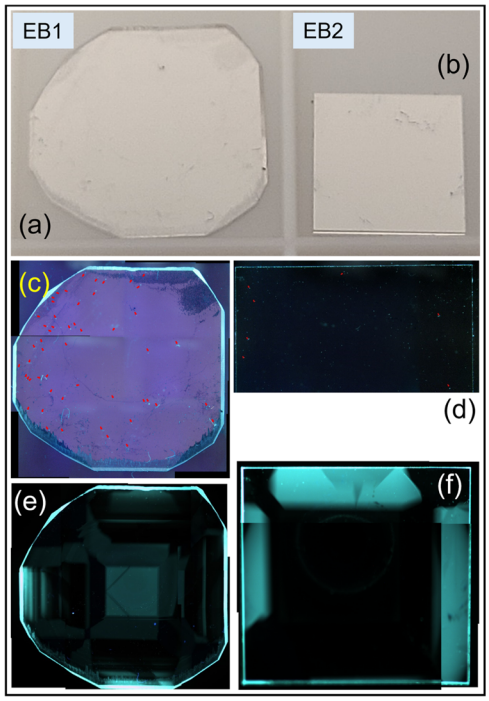

Figure 1. a,c, and e) Photos of samples EB; b,d, and f) EB2 under illumination with a,b) visible light; c and d) cross-polarized light; and e and f) DUV light at photon energy above 5.51 eV. Red arrows (c and d) show locations of macroscopic metallic inclusions inside diamond. Dark regions near edges of EB1 (c) correspond to unpolished areas.

The SPV signals were coupled out with a charge amplifier. The distance between the electrode and the sample surface was adjusted with a test signal.

The in-phase (X) and phase-shifted by 90° (Y) signals were obtained by multiplying the time (t) dependent signals with $\sin(2\pi \cdot t/T_{\mathrm{mod}})$ and $\cos(2\pi \cdot t/T_{\mathrm{mod}})$, respectively, and integrating over $40 \cdot T_{\mathrm{mod}}$ and normalizing to $40 \cdot T_{\mathrm{mod}}$ after integration Equations (4) and (5).

$$X = {}^{1}/_{40} \cdot T_{\mathrm{mod}} \cdot \int_{0}^{40 \cdot T_{\mathrm{mod}}} \mathrm{SPV}(t) \cdot \sin(2\pi \cdot t/T_{\mathrm{mod}}) \cdot \mathrm{d}t \tag{4}$$

$$Y = {}^{1}/_{40} \cdot T_{\mathrm{mod}} \cdot \int_{0}^{40 \cdot T_{\mathrm{mod}}} \mathrm{SPV}(t) \cdot \cos(2\pi \cdot t/T_{\mathrm{mod}}) \cdot \mathrm{d}t \tag{5}$$

The X and Y signals can be assigned to the fast and slow responses in relation to T_{mod}. For example, if the SPV signals increase and decrease within times much shorter than T_{mod}, the Y signal is zero. In contrast, if the SPV signals increase and decrease within times much longer than T_{mod}, the X signal is zero (see also Figure S2, Supporting Information).

The spectrum of $\phi(h\upsilon)$ was previously measured[15] and $D(h\upsilon)$ was approximated by:

$$D(h\upsilon) = \int_{h\upsilon-2.2\cdot\Delta E}^{h\upsilon+2.2\cdot\Delta E} \exp\left(-\left(\frac{E}{\Delta E}\right)^2\right) \mathrm{d}E \tag{6}$$

where $\Delta E(h\upsilon)$ is the spectral line width of the DPM100 monochromator, which was recently published.[15] The shape of the spectrum of $\Delta E(h\upsilon)$ was fitted with the following expression

$$\Delta E(h\upsilon) = 0.6\mathrm{eV} \cdot \left[\frac{0.087 \cdot \exp(-\frac{h\upsilon-1.1\mathrm{eV}}{3.2\mathrm{eV}})}{1+\exp(-\frac{h\upsilon-1.01\mathrm{eV}}{0.22\mathrm{eV}})} + 0.012 \cdot \exp\left(-\left(\frac{h\upsilon-1.4\mathrm{eV}}{0.9\mathrm{eV}}\right)^2\right)\right] \tag{7}$$

In modulated SPV spectroscopy, the signals shall be fast enough to follow the modulation period, i.e., separation of photogenerated charge carriers and recombination dominate during light-on and light-off half-periods, respectively. Depending on the mechanisms of charge carrier dynamics, the response times for charge separation and recombination can vary over many orders of magnitude (limitations, for example, by the dielectric relaxation time or by thermal excitation).[12] In doped conventional semiconductors, such as Si or GaN, the drift of photogenerated charge carriers in depletion regions causes very short times for charge separation, whereas thermal excitation of minority charge carriers leads to slow recombination dynamics of charge carriers separated in space. Charge separation in undoped diamond is driven by asymmetric trapping of diffusing charge carriers at surface states and thermal excitation limits the recombination dynamics. Regarding to,[12,15] the sensitivity of the method can be illustrated by assuming a moderate charge separation (or diffusion) length of about 1 µm and a sensitivity limit of the order of µV. In such case, the separation and recombination of about $10^5\,\mathrm{cm}^{-2}\,\mathrm{s}^{-1}$ charge carriers should follow the modulation for getting modulated SPV signals. For comparison, the photon flux of the given set-up is of the order of $10^{14}...10^{15}\,\mathrm{cm}^{-2}\,\mathrm{s}^{-1}$, i.e., the absorption of a tiny part of incoming photons by defects is sufficient for generating modulated SPV signals under sufficient charge separation and recombination.

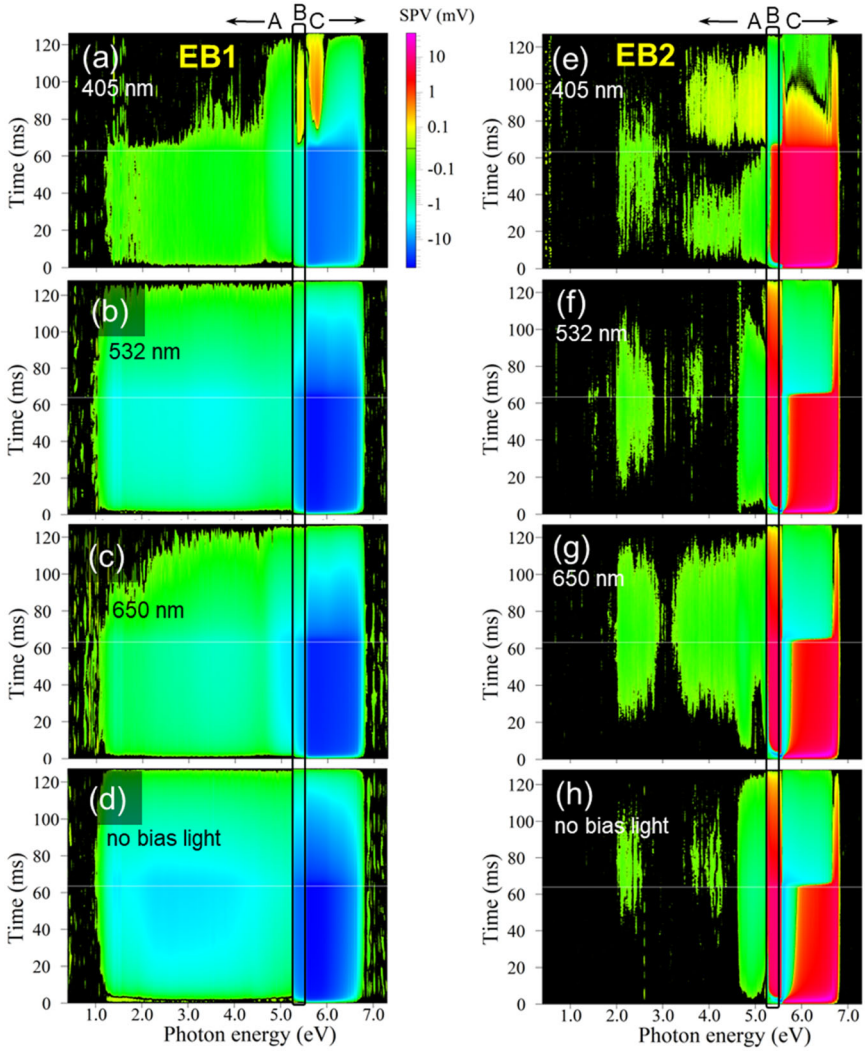

Figure 2. Contour plots over the first (light on) and second (light off) halves of the modulation period for samples a–d) EB1 and e–f) EB2 measured under bias light of 405 nm a and e), 532 nm, b and f) and 650 nm, c and g) and measured without bias light, and d and h). A, B, and C mark the regions of defect-related transitions, transitions dominated by exciton dissociation (between 5.26 and about 5.5 eV) and strong absorption (above 5.5 eV).

3. Results and Discussions

Figure 2 shows the contour plots for samples EB1 and EB2 measured under bias light illumination and measured without bias light. For modulated transient spectroscopy, a contour plot represents a map of positive and negative SPV signals on logarithmic color scales as a function of photon energy and time whereas the modulated light was on (first half of T_{mod}) and off (second half of T_{mod}).

The contour plots of samples EB1 and EB2 behave very differently. The SPV signals of sample EB1 are negative over the entire spectral range and T_{mod}, excepting two narrow regions between about 5.2 and 5.7 eV where positive signals appeared during the second half period under bias illumination at 405 nm. Positive and negative signals appeared for sample EB2 independent of bias illumination. Maximum negative and positive signals of up to −50 and +30 mV were reached for samples EB1 and EB2, respectively, under strong absorption. For samples EB1 and EB2, SPV signals set on at about 1 and 2 eV, respectively. The structure of the contour plots depended on bias illumination. However, a precise description of onset energies is not straightforward.

Figure 3, **4** show the *X* and *Y* spectra deduced from the contour plots at photon energies below 5.2 eV (defect range) for samples EB1 (Figure 2) and EB2 (Figure 4). The local extrema in the spectra of sample EB1 around 1.4 eV are related to the lamp spectrum. The spectra were measured with and without bias light. For sample EB1, bias light led to a general decrease in modulated SPV signals. In contrast, spectral features appeared more pronounced under bias light for sample EB2.

The determination of onset energies is not straightforward for the analysis of the rather broad spectra of sample EB1. Numerous changes of the slopes appeared for the Y spectrum of sample EB1 under bias light at 532 nm, for example, around 1.01, 1.2, 1.7, 1.89, 2.09, 2.27, 2.5, 2.6, 2.87, 3.38, 3.79, 4.49, and

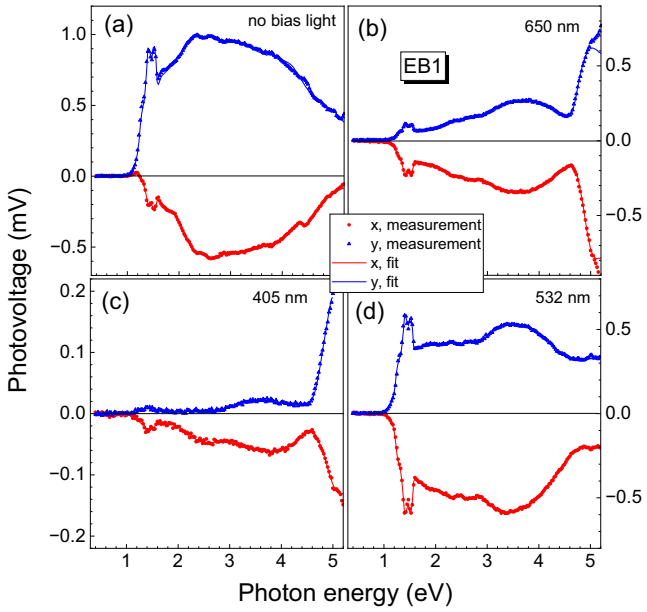

Figure 3. X (red circles)- and Y (blue triangles)-spectra in the defect range of sample EB1 measured a) without bias light and under bias light at b–d) 650, 532, and 405 nm, respectively in the range of photon energies below 5.2 eV. The red and blue lines are fits with respect to Equation (2).

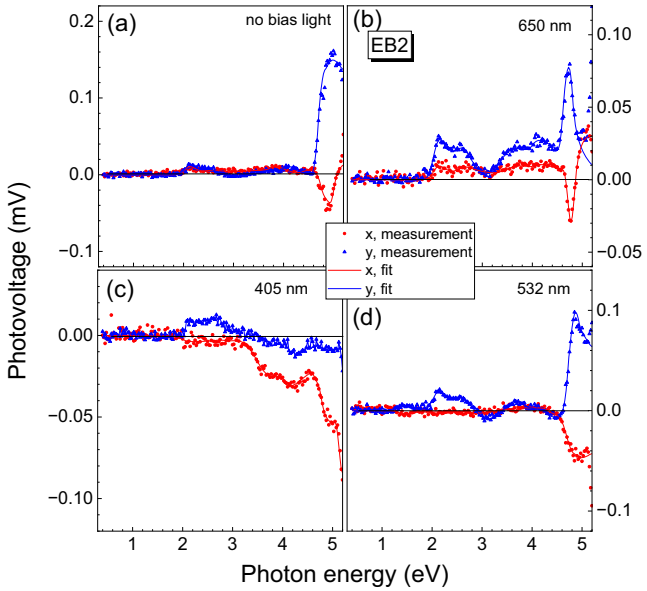

Figure 4. X (red circles)- and Y (blue triangles)-spectra in the defect range of sample EB2 measured a) without bias light and under bias light at b–d) 650, 532, and 405 nm, respectively in the range of photon energies below 5.2 eV. The red and blue lines are fits with respect to Equation (2).

4.84 eV, whereas it is unclear which changes of the slopes correspond to transition energies and whereas transitions are hidden in the range between about 1.25 and 1.6 eV where lines of the lamp spectrum are prominent. The situation is rather similar for sample EB2, for which changes of the slopes appeared for the *Y* spectrum under bias light at 650 nm, for example, around 1.94, 2.13, 2.4, 2.6, 2.79, 3.09, 3.48, 3.95, 4.47, and 4.75 eV. Here, for example, it is not clear whether the changes in the slopes arose due to the onset of characteristic defect transitions or due to the partial overlap of positive and negative signal contributions.

In the following, the spectra will be analyzed with respect to the effective absorption cross section (Equation 2). The *X* and *Y* signals were zero (or equal to the noise) at the lowest (between 0.4 and 0.5 eV) and highest (between 6.8 and 7.3 eV) photon energies since there was no photon flux in these regions. Values of $E_{abs,i}$, $\sigma_{abs,i}$, and A_i could not be fitted by one general algorithm due to rather different amplitudes and overlap of positive and negative signals. The fitting of the effective absorption cross sections started from the lowest photon energy. The starting values of the corresponding $E_{abs,1}$, $\sigma_{abs,1}$, and A_1 were set to values close to the maximum slope of the increasing positive or negative signals, to the approximate range of the increase up to the maximum slope and to an amplitude about 2 times higher than the signal at the maximum slope, respectively. In the following, $E_{abs,1}$, $\sigma_{abs,1}$, and A_1 were fitted until the difference between the measured and fitted spectra allowed for the definition of starting values for $E_{abs,2}$, $\sigma_{abs,2}$, and A_2 from the onset of the difference spectrum and so on. For the fitting procedure, a software was developed allowing for manual fitting, generating starting values.

As an example, **Figure 5** shows a fit sequence of Y signals of sample EB2 under bias light at 650 nm. The fits started from the lowest photon energy and the number of transitions increased from $n = 1$ (Figure 5a) to $n = 8$ (Figure 5h). The first onset range could be well fitted with an absorption energy of 2.00 eV. The positive signals of the first contribution were significantly larger than the measured signals. The corresponding positive signals of the first contribution were partially compensated by the negative signals of the second contribution, so that the range around the second onset energy was well fitted. For the second onset energy, an effective optical cross section with an absorption energy of 2.12 eV was obtained. The procedure of fitting the parts of the spectra nearest to the absorption energy of the previous contribution was repeated until the *Y* spectrum was fitted over the entire defect range. For the *Y* spectrum of sample EB2 under bias light at 650 nm, a minimum of eights contributions was needed for the fit. In contrast, 10 changes of the slopes could be distinguished in the case of a conventional analysis. Therefore, the conventional analysis of transition energies is not suitable for the interpretation of rather complex modulated SPV spectra, such as for HPHT diamond. Furthermore, the remaining residuals, setting on at about 5 eV were fitted with an exponential (up to about 5.2 eV), whereas the energy of the exponential tails was 0.07 eV.

The similar fit procedure was applied for all measured *X* and *Y* spectra (see the thin lines in Figure 3 and 4). For sample EB1, the fits were started with the *X* and *Y* spectra under bias light at 405 nm since these spectra showed the clearest features with the lowest number of changes in the slopes. The absorption energies obtained from these fits were then used as starting values for the fits of the other spectra, whereas additional defect transitions could appear and absorption energies could change as well.

As a general example, **Figure 6**a shows the measured and fitted spectra of the *Y* signals under bias light at 532 nm and the

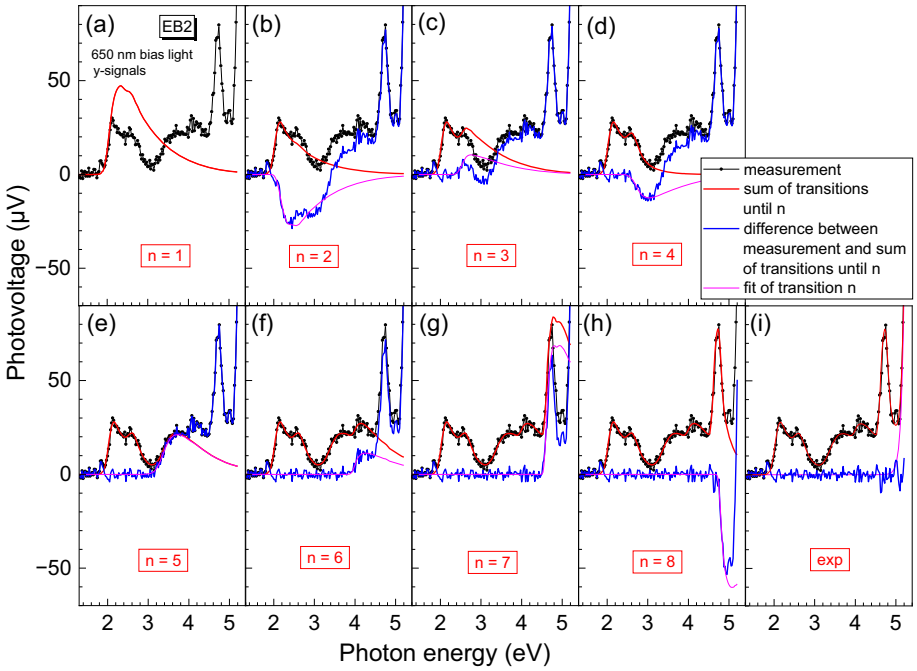

Figure 5. Example for a fit sequence of Y signals of sample EB2 under bias light at 650 nm with respect to Equation (2) starting from the lowest photon energy and increasing the number of transitions from a) $n = 1$, b–g) via $n = 2$–7, and h) to $n = 8$ and implementing an exponential at highest photon energies. Eight defect transitions were necessary for the complete fit of the given example up to about 5 eV.

contributions of the 10 transitions that were needed for the fit. The corresponding values of $E_{abs,i}$ amounted to 0.96, 1.14, 1.44, 1.68, 2.10, 2.51, 3.06, 3.72, 4.49, and 4.87 eV. Incidentally, the error of the values of $E_{abs,i}$ is of the order of 10–20 meV (see also Figure S4, Supporting Information).

As a further example, Figure 6b shows the measured and fitted spectra for sample EB2 of the *Y* signals under bias light at 650 nm and the contributions of the 8 transitions which were needed for the fit as a minimum. The corresponding values of $E_{abs,i}$ amounted to 2.00, 2.12, 2.48, 2.68, 3.33, 3.95, 4.57, and 4.76 eV. Incidentally, transitions above 5 eV were not considered in the fit.

The transitions at 0.96, 1.14, 1.44, and 1.68 eV, which were present in sample EB1, were not observed in sample EB2. The absorption energies of 2.10, 2.51, 4.49, and 4.87 eV observed in sample EB1 were close to the values of 2.12, 2.48, 4.57, and 4.76 eV found in sample EB2 whereas the corresponding broadening parameters were much smaller for sample EB2. It is reasonable to relate these four transitions to defects with the same nature. The absorption energies of 3.06 and 3.72 eV appeared in sample EB1 but not in sample EB2. Furthermore, the absorption energies of 2.68, 3.33, and 3.95 eV were detected in sample EB2 but not in sample EB1. For comparison, an increase of absorption set on at about 2.2 eV and broad absorption bands centered around 3.3 and 4.5 eV appeared in Ib HPHT diamond.[16] Rosa et al. assigned defects in CVD diamond with photoionization energies of 1.2 and 2.2 eV to hydrogen-related bulk defects and to a substitutional nitrogen defect state, respectively.[17] Gaubas et al. found photoactivation energies at 0.52, 0.74, 1.1, 1.5, 2.0, 2.7, and 4.0 eV in HPHT diamond.[18]

Incidentally, the quality of the fits depended on the sample and on the bias light, as can be seen from the residual sum of squares (RSS). The values of RSS were obtained between 0.4 and 5.0 eV and are summarized in Figure S3, Supporting Information. The highest RSS was obtained for the broad spectrum with scarce structures of the Y signals of sample EB1. The RSS values decreased with decreasing wavelength of the bias light since defect transients appeared more pronounced.

Figure 7 shows the effective absorption cross sections of defect transitions, which were extracted from the fits of the *Y* signals of samples EB1 under bias light at 532 nm and EB2 under bias light at 650 nm. The effective absorption cross sections of sample EB1 were dominated by the broad defect transition with the absorption and broadening parameters of 3.06 and 0.39 eV, respectively. For the transitions at 2.10 and 2.51 eV (sample EB1) and 2.12 and 2.48 eV (sample EB2), the values of ($\sigma_{abs,eff,i}$) were larger by about 5 times for sample EB1 than for sample EB2. For the transitions at 4.49 and 4.87 eV (sample (EB1) and 4.57 and 4.76 eV (sample (EB2), the values of ($\sigma_{abs,eff,i}$) were also larger for sample EB1.

Aside from absorption cross sections of defects, transition energies also depend on occupation in SPV measurements. For example, under modulated excitation, the occupation of a defect state can depend on time, i.e., *X* and *Y* signals may be related to different occupations. Furthermore, the occupation of defect states was changed by bias light. Here, it shall be remarked that only qualitative changes were considered for this study and that the systematic variation of the occupation of defect states is beyond the scope of this work.

Absorption energies extracted for X and Y signals ($E_{abs,X}$ and $E_{abs,Y}$, respectively) of samples EB1 and EB2 are correlated with

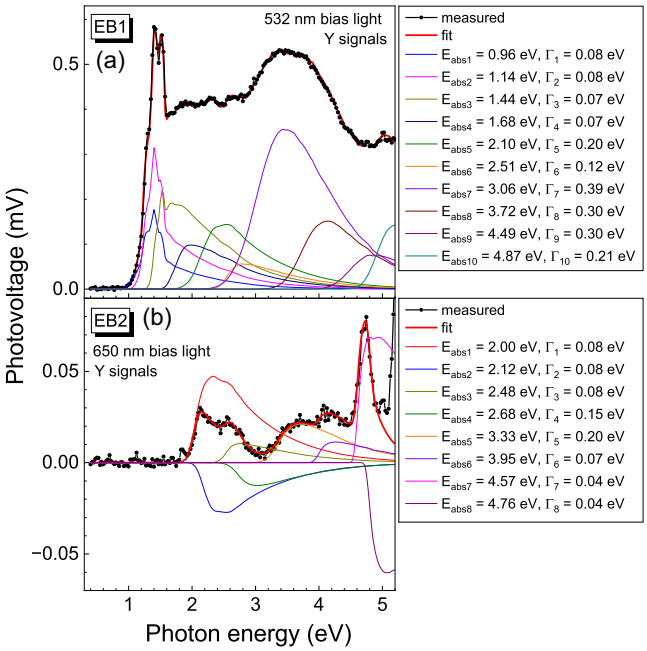

Figure 6. Example for the measured (black circles) and fitted (thick red line) spectrum of the Y signals of sample a) EB1 under bias light at 532 nm and b) of sample EB2 under bias light at 650 nm and for the contributions of the transitions which were necessary for the fit of sample EB1 ($E_{abs,i}$ = 0.96, 1.14, 1.44, 1.68, 2.10, 2.51, 3.06, 3.72, 4.49, and 4.87 eV (thin blue, magenta, dark yellow, navy, olive, orange, violet, wine, purple, and dark cyan lines, respectively)) and of sample EB2 ($E_{abs,i}$ = 2.00, 2.12, 2.48, 2.68, 3.33, 3.95, 4.57, and 4.76 eV (thin red, blue, dark yellow, olive, orange, violet, magenta, and purple lines, respectively)). The boxes at the right side give also the corresponding values of the broadening parameters (Γ_i).

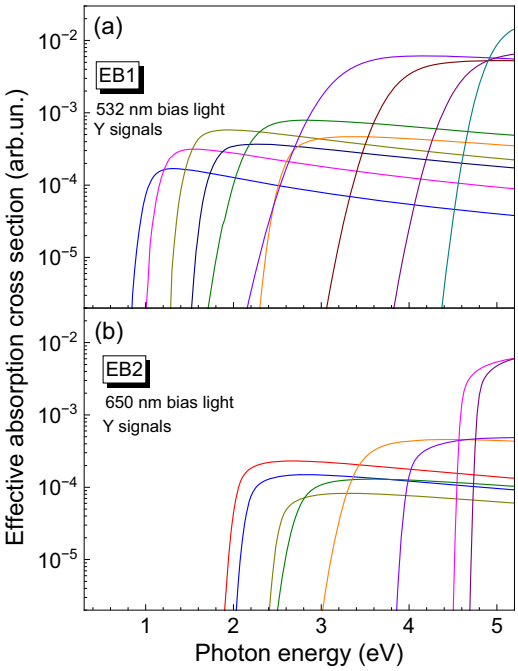

Figure 7. Effective absorption cross sections of defect transitions extracted from the fits of the Y signals of samples a) EB1 under bias light at 532 nm for the contributions with the absorption energies $E_{abs,i}$ = 0.96, 1.14, 1.44, 1.68, 2.10, 2.51, 3.06, 3.72, 4.49, and 4.87 eV (thin blue, magenta, dark yellow, navy, olive, orange, violet, wine, purple, and dark cyan lines, respectively) and b) EB2 under bias light at 650 nm for the contributions with the absorption energies $E_{abs,i}$ = 2.00, 2.12, 2.48, 2.68, 3.33, 3.95, 4.57, and 4.76 eV (thin red, blue, dark yellow, olive, orange, violet, magenta, and purple lines, respectively).

each other for measurements without and with bias light in **Figure 8**. Incidentally, not all transitions were unambiguously detected in both spectra of X and Y signals, i.e., some transitions might be missing, what was the case, for example, between 4 and 4.6 eV for sample EB1. Therefore, one has to keep in mind that the analysis of modulated SPV spectra by using Equation (2) can still bear some uncertainties.

For sample EB1, $E_{abs,X}$, and $E_{abs,Y}$ were nearly identical at energies below 4 eV, i.e., thedynamics of charge separation and relaxation were rather similar. In contrast, $E_{abs,Y}$ was less than $E_{abs,X}$ in several cases at photon energies above 4 eV. The red arrows mark characteristic defect transitions in Figure 8. Transitions around 1.00, 1.45, 2.12, 3.1, and 4.8 eV were present under all measurement conditions for sample EB1, whereas values of $E_{abs,X}$ and $E_{abs,Y}$ did scatter, for example, over up to 0.1 eV for 1.45 and 0.2 eV for $E_{abs,Y}$ around 4.8 eV. Transitions around 1.2, 1.68, 2.56, 3.67, and 4.3 eV were present, not for all measurement conditions, for example, transitions around 1.2, 1.68, 2.56, and 3.67 eV were only absent under bias light at 405 nm.

For sample EB2, the values of $E_{abs,X}$ and $E_{abs,Y}$ did scatter strongly than for sample EB1. This is not surprising since the signal-to-noise ratio was much smaller for sample EB1 than for sample EB2. Furthermore, four transitions appeared around 2.00, 2.12, 2.48, and 2.66 eV for sample EB2. In contrast, two transitions were sufficient for the fits of sample EB1 in this range. The transition with E_{abs} around 1.35 eV was very weak and appeared only under bias light at 532 nm.

In the following, the transition energies $E_{abs,i}$ measured by modulated SPV spectroscopy are compared with related empirical data obtained by absorption or photoelectric spectroscopy, such as photocurrent or constant photocurrent measurements (PC or CPM) or optically detected deep level transient spectroscopy (ODTS), and with specific transition energies obtained by density functional theory (DFT) analysis. It shall be noted that a direct comparison with luminescence data is not possible due to the different role of Stokes shifts. Furthermore, one should keep in mind that the assignment of $E_{abs,i}$ to a certain transition may be rather speculative without more detailed experimental work. Absorption lines have been carefully studied in diamond gems.[19–21] Nitrogen was present in both crystals. The substitutional nitrogen donor in diamond is 1.7 eV below the conduction band edge.[22] CPM data showed absorption bands at 1.6, 4.0, and 4.7 eV on nominally undoped diamond and at 2.4 and 4.7 eV in nitrogen-rich diamond,[23] whereas broad absorption bands at 1.0, 2.3, 3.0, and 4.2 eV were observed as well in nitrogen-doped diamond.[24] Nesládek et al. interpreted broad absorption features below the bandgap of diamond by transitions caused by sp2 hybridization (π–π^*, peak energies between 2.9 and 3.4 eV depending on the sample) and by transitions from

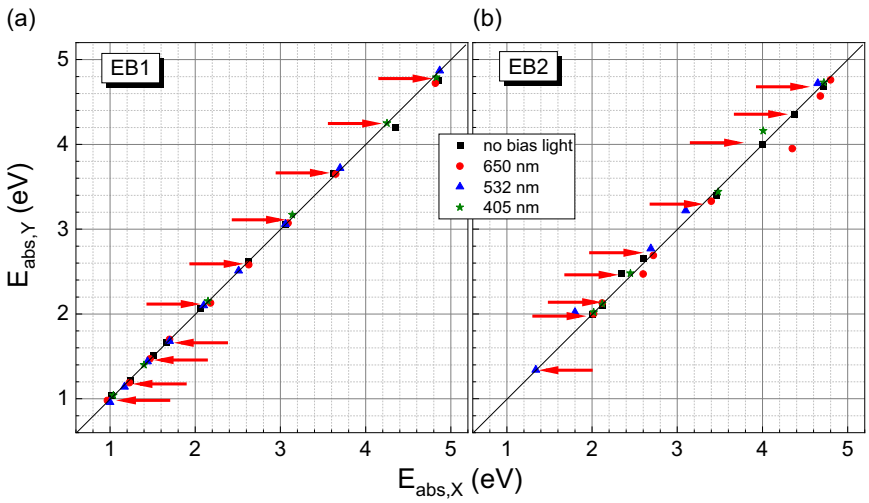

Figure 8. Summary of the absorption energies of defect transitions in samples a) EB1 and b) EB2 obtained from the fits of the spectra of the X and Y signals measured without bias light (black squares) and under bias light at 650, 532, and 405 nm (red circles, blue triangles and olive stars, respectively). The red arrows mark characteristic regions of defect transitions for $E_{abs,Y}$.

sp2 orbitals into the conduction band (π-Σ^*, peak energies between 3.62 and 4.45 eV depending on the sample).[25] Features with onsets at 1.3 and 2.2 eV in PC spectra were attributed to a hydrogen-related defect and the single-substitutional nitrogen defect, respectively.[26] Two excitation energies at 0.9 and 1.25 eV were distinguished by ODTS, whereas the transition at 1.25 eV was ascribed to the positively charged vacancy.[27] DFT analysis of charged nitrogen impurity defects showed, for example, transitions at about 1.8 and 4.4 eV above the valence band for the negatively charged NV complex and at about 4.8 eV above the valence band for the positively charged N^+ defect.[28] Silicon can form complexes with vacancies and hydrogen having for example, electronic states at about 1 and 5 eV above the valence band as found by DFT analysis.[29] Nickel can play an important role in the formation of defects in HPHT diamond. A broad absorption band near 1.4 eV and a series of absorption lines near 3.1 eV were associated with nickel-related optical centers.[30] It was shown that the Ni-acceptor has an energy level of about 2.0 eV above the valence band.[31] Nickel complex defects were found by DFT analysis, for example, at 1.71, 2.17, 2.71, and 4.18 eV above the valence band.[32] It was shown by DFT analysis that oxygen related defects can have positions, for example, in the ranges of 3.6 eV above the valence band or 2.6 and 1.4 eV below the valence band.[33] The onset at about 5 eV (see Figure 4) can be explained by boron acceptors.[24] **Table 2** summarizes the values of $E_{abs,i}$ and gives possible assignments to defects. It is worth to note that SPV spectroscopy is highly sensitive to electronic and charge-related defect states, even if those defects are "dark" (nonfluorescent), making it powerful for locating and characterizing nonfluorescent or shallow electronic traps near the surface. However, it also makes difficult a direct assignment of "dark" defect without complimentary techniques. Furthermore, it shall be pointed out that fluorescence and/or absorption spectroscopies can be complementary to modulated SPV spectroscopy since excited charge carriers are not necessarily separated in space. Incidentally, the extracted $\sigma_{abs,eff,i}$ values are of the same order as values of the full width of half maximum (FWHM) for defect transitions obtained by CPM (see, for example,).[23,26]

Table 2. Absorption energies of observed transitions in samples EB1 and EB2 and possible assignments to defects.

	EB1 $E_{abs,i}$ [eV]	Possible assignment	EB2 $E_{abs,i}$ [eV]	Possible assignment
1	1.01	Si-V:H[29]	–	
2	1.14	Si-V:H2[29] a-C[18]	–	
3	1.22	N-V-N[20] V^+[27]	–	
4	1.46	O related[33]	1.34	H-related[26]
5	1.69	N_s[22] V^0[20]	–	
6	–		2.01	NV^-[20,28]
7	2.12	N_s[26] NV^0[20]	2.12	N_s[26]$NV^{0/-}$
8	–		2.47	N related[23] 4 N+2 V[20]
9	2.6	O related[33] Ni_sVN_s[32]	2.69	N_2V^0[20]
10	3.06	3 N+V[20] π-π^*[25]	–	
11	–		3.33	Ni_s^-[31]
12	3.66	O related[33]	3.44	Ni_s^-[31]
13	–		4.01	N related[25]
14	4.25	Si-V:H,H_2[29]	–	
15	–		4.4	NV^-[28]
16	–		4.65	N related[23]
17	4.82	N^+[28]	4.78	N^+[28]

The defect transitions fit developed in this work is a general approach allowing for fitting any absorption spectra in defect

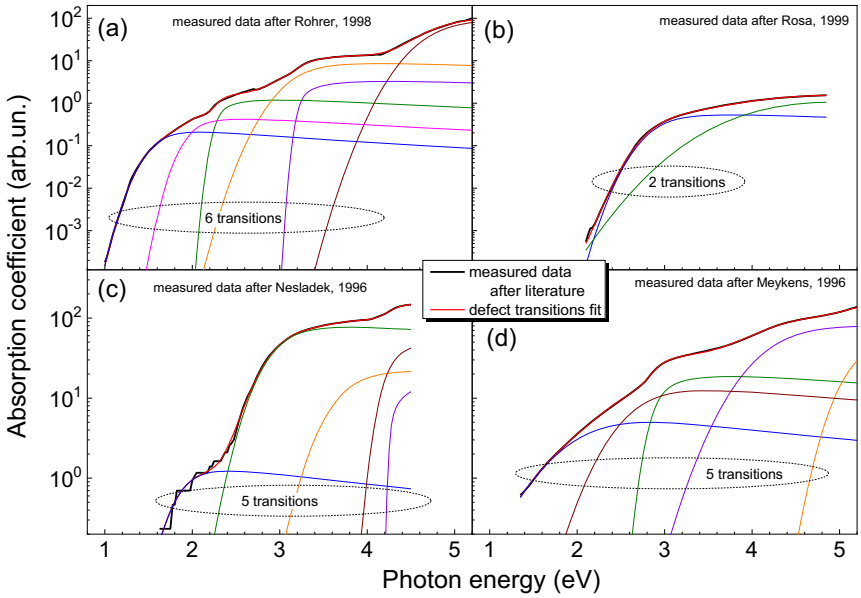

Figure 9. Defect transitions fits (red lines) of measured absorption spectra (data after literature, thick black lines) for spectra shown in a),[24] b),[17] c),[25] and d)[16]. The thin colored lines mark the effective absorption cross sections of transitions contributing to the overall absorption spectrum.

regions. Advantages of fitting absorption spectra are that there are no changes of the sign in the difference to modulated SPV spectra and that (effective) absorption cross sections are directly related to the absorption spectra, i.e., without an uncertainty between regions in which absorption and charge separation take place, as can be in SPV measurements. In the past, absorption spectra of diamond were obtained mainly from CPM and photohermal deflection spectroscopy (PDS) measurements. As an example, **Figure 9**a–d show some measured absorption spectra deduced from data published in literature in the 90ies and corresponding defect transitions fits with a minimum of defect transitions necessary for a satisfactory fit. Incidentally, a satisfactory fit means that the quality of the fit does not improve significantly if further increasing the number of transitions.

In the past, absorption spectra could not be so well fitted. For example, some authors characterized defect transitions via onset energies, in some cases even in logarithmic plots. In contrast to previous works, the values of $E_{abs,i}$ and Γ_i can be obtained with high accuracy over the overall measured absorption spectra by applying the procedure of defect transitions fit developed in this work. The numbers of transitions necessary for satisfactory fits are given in the Figure 9a–d and the corresponding values of $E_{abs,i}$, Γ_i and A_i are summarized in **Table 3**. Striking differences appeared in number of transitions and transition energies given by the authors and obtained by the defect transitions fit. This shows that the application of defect transitions fit opens a new way for a detailed analysis and therefore for a new interpretation of previously measured data.

Table 3. Defect transition parameters obtained from the fits shown in figure 9 and values of transition energies from original papers.

Diamond type	Defect transitions fit		Transition energies from reference [eV]	Reference of absorption spectrum
	$E_{abs,i}$ [eV]	Γ_i [eV]		
CVD, 57 µm	1.52	0.23	1.0	[24]
	1.92	0.20	2.3	
	2.25	0.09	3.0	
	3.08	0.34	4.2	
	3.19	0.07		
	4.61	0.38		
CVD, annealed and oxidized	2.80	0.31	2.2	[17]
	3.83	0.72		
HPHT, Ib	1.77	0.25	–	[25]
	2.82	0.31		
	3.55	0.33		
	4.15	0.14		
	4.25	0.04		
Flame grown on {110} natural diamond, IIa	1.92	0.61	2.2	[16]
	2.52	0.45	3.3	
	2.82	0.15	4.5	
	4.01	0.51		
	5.01	0.29		

4. Conclusions

It has been shown that the rather complex modulated SPV spectra of HPHT diamond can be well fitted by taking into account a sum of absorption (or photogeneration) cross sections of defects. This means that the SPV signals correspond to the small signal case and that the charge separation and relaxation processes related to photogeneration from the different defects are independent of each other. Up to ten absorption energies and broadening parameters were obtained over the entire bandgap of diamond, depending on preparation. It was shown that the application of bias light can be used to suppress or enhance certain transitions,

giving the opportunity for more detailed analysis of the role of the photogeneration rate in the future. Our general approach of SPV analysis opens a new perspective for contactless photoelectric characterization of defects not only in diamond but also in other photoactive materials. In addition, the developed fitting procedure is applicable for the precise characterization of defect transitions in the absorption spectra of any semiconductor.

Supporting Information

Supporting Information is available from the Wiley Online Library or from the author.

Acknowledgements

S.F. and T.D. are grateful to Dr. K. Dornich (Freiberg Instruments) and Prof. T. Petit (Helmholtz-Zentrum Berlin) for promoting the project. Furthermore, the authors are very grateful to the reviewers for detailed and inspiring questions.

Open Access funding enabled and organized by Projekt DEAL.

Conflict of Interest

The authors declare no conflict of interest.

Data Availability Statement

The data that support the findings of this study are available from the corresponding author upon reasonable request.

Keywords

absorption cross sections, defects, diamonds, high pressure high temperature, surface photovoltage spectroscopy

Received: June 29, 2025
Revised: September 24, 2025
Published online:

[1] C. D. Clark, P. J. Dean, P. V. Harris, *Proc. R. Soc. Lond. A* **1964**, *277*, 312.
[2] S. Ghosh, H. Surdi, F. Kargar, F. A. Koeck, S. Rumyantsev, S. Goodnick, R. J. Nemanich, A. A. Balandin, *Appl. Phys. Lett.* **2022**, *120*, 062103.
[3] R. S. Balmer, I. Friel, S. M. Wollard, C. J. H. Wort, G. A. Scarsbrook, S. E. Coe, E. El-Hajj, A. Kaiser, A. Denisenko, E. Kohn, J. Isberg, *Phil. Trans. R. Soc. A* **2008**, *366*, 251.
[4] Z. Han, C. Bayram, *IEEE Electr. Dev. Lett.* **2023**, *44*, 1692.
[5] F. Zhao, Y. He, B. Huang, T. Zhang, H. Zhu, *Materials* **2024**, *17*, 3437.
[6] T. Shimaoka, S. Koizumi, J. H. Kaneko, *Func. Diamond* **2021**, *1*, 205.
[7] J. Rovny, S. Gopalakrishnan, A. C. B, Jayich, P. Maletinsky, E. Demler, N. P. de Leon, *Nat. Rev. Phys.* **2024**, *6*, 753.
[8] L.-X. Su, Y. Cao, H.-S. Hao, Q. Zhao, J. Zhi, *Funct. Diamond* **2021**, *1*, 93.
[9] S. S. Dossa, I. Ponomarev, B. N. Feigelson, M. Hainke, C. Kranert, J. Friedrich, J. J. Derby, *J. Cryst. Growth* **2023**, *609*, 127150, and references therein.
[10] See for example, B. L. Green, A. T. Collins, C. M. Breeding, *Rev. Mineral. Geochem.* **2022**, *88*, 637.
[11] L. Kronik, Y. Shapira, *Surf. Sci. Rep.* **1999**, *37*, 1.
[12] T. Dittrich, S. Fengler, *Surface Photovoltage Analysis Of Photoactive Materials*, World Scientific, New Jersey, London, Singapore, Beijing, Shanghai, Hong Kong, Taipei, Chennai, Tokyo **2020**.
[13] A. Alkauskas, M. D. McCluskey, C. G. Van de Walle, *J. Appl. Phys.* **2016**, *119*, 181101.
[14] T. Dittrich, S. Fengler, *Phys. Status Solidi RRL* **2025**, 2400384, https://doi.org/10.1002/pssr.202400384.
[15] T. Dittrich, S. Fengler, M. Franke, *Appl. Opt.* **2024**, *63*, 6880.
[16] K. Meykens, M. Nesládek, C. Quaeyhaegens, L. M. Stals, M. Vaněček, J. Rosa, G. Janssen, J. J. Schermer, *Diamond Relat. Mater.* **1996**, *5*, 958.
[17] J. Rosa, M. Vaněček, M. Nesládek, L. M. Stals, *Diamond Relat. Mater.* **1999**, *8*, 731.
[18] E. Gaubas, T. Ceponis, D. Meskaukaite, R. Grigonis, V. Sirutkaitis, *JINST* **2016**, *11*, C01017.
[19] A. T. Collins, *Diamond Relat. Mater.* **2003**, *12*, 1976.
[20] J. E. Shigley, C. M. Breeding, *Gems Gemol.* **2013**, *49*, 107.
[21] T. Hainschwang, F. Notari, G. Pamies, *Minerals* **2020**, *10*, 914.
[22] R. G. Farrer, *Solid State Commun.* **1969**, *7*, 685.
[23] R. Rohrer, C. F. O. Graeff, R. Janssen, C. E. Nebel, M. Stutzmann, *Phys. Rev. B* **1996**, *54*, 7874.
[24] R. Rohrer, C. E. Nebel, M. Stutzmann, A. Flöter, R. Zachai, X. Jiang, C.-P. Klages, *Diamond Relat. Mater.* **1998**, *7*, 879.
[25] M. Nesládek, K. Meykens, L. M. Stals, M. Vaněček, J. Rosa, *Phys. Rev. B* **1996**, *54*, 5552.
[26] M. Nesládek, L. M. Stals, A. Stesmans, K. Iakubovsky, G. J. Anriaenssens, J. Rosa, M. Vaněček, *Appl. Phys. Lett.* **1998**, *72*, 3306.
[27] C. E. Nebel, R. Zeisel, M. Stutzmann, *Diamond Relat. Mater.* **2001**, *10*, 639.
[28] R. Löfgren, K. V. Sopiha, S. Öberg, J. A. Larsson, *Comp. Mater. Sci.* **2025**, *250*, 113685.
[29] G. Thiering, A. Gali, *Phys. Rev. B* **2015**, *92*, 165203.
[30] A. T. Collins, H. Kanda, R. C. Burns, *Phil. Mag. B* **1990**, *61*, 797.
[31] T. Chanier, A. Gali, *Phys. Rev. B* **2013**, *87*, 245206.
[32] T. Fujimura, T. Yamasaki, K. Manabe, H. Momida, *Diamond Relat. Mater.* **2022**, *128*, 109280.
[33] G. Thiering, A. Gali, *Phys. Rev. B* **2016**, *94*, 125202.